IMA Journal of Numerical Analysis (2026) **00**, 1–25
https://doi.org/10.1093/imanum/drag046

Projection-free Gauss methods for harmonic maps

GEORGIOS AKRIVIS
Department of Computer Science and Engineering, University of Ioannina, 451 10 Ioannina, Greece, and Institute of Applied and Computational Mathematics, FORTH, 700 13 Heraklion, Crete, Greece

JIASHUN HU
Department of Applied Mathematics, The Hong Kong Polytechnic University, Hong Kong, China

AND

JILU WANG*
School of Science, Harbin Institute of Technology, Shenzhen 518055, China
*Corresponding author: wangjilu@hit.edu.cn

[Received on 21 July 2025; revised on 1 April 2026; accepted on 1 April 2026]

We construct and study projection-free Gauss methods for harmonic maps into spheres, extending the Crank–Nicolson scheme to arbitrarily high order. Existing projection-free methods are limited to second-order accuracy; in contrast, our schemes attain high-order temporal accuracy while preserving the unit-length constraint and ensuring discrete energy dissipation unconditionally. We furthermore introduce practical linearized variants of the base schemes via fixed-point iteration, which preserve the constraint up to machine precision when sufficiently iterated, and achieve higher-order accuracy in the constraint violation even with a fixed number of iterations. Numerical experiments demonstrate that the proposed methods maintain high temporal accuracy and effectively control the constraint violation; notably, preserving the unit-length constraint up to machine precision enables highly accurate steady-state computations with large time steps, highlighting the robustness and efficiency of the methods.

Keywords: Harmonic maps; Gauss methods; collocation methods; energy-decay property; unit-length property; fixed-point iteration.

1. Introduction

Harmonic maps into spheres arise as a canonical example of constrained variational problems and are the critical points of the Dirichlet energy functional,

$$I(u) = \frac{1}{2}\int_{\Omega} |\nabla u|^2 \,\mathrm{d}x, \tag{1.1}$$

among all vector fields $u = (u^1, \dots, u^\ell) : \Omega \to \mathbb{S}^{\ell-1}$, subject to Dirichlet boundary conditions, $u|_{\Gamma_{\mathrm{D}}} = u_{\mathrm{D}}$, for a given function u_{D} which is assumed to be equal to the trace of a function $\tilde{u}_{\mathrm{D}} \in H^1(\Omega; \mathbb{S}^{\ell-1})$. Here, $\Omega \subset \mathbb{R}^d$ is a bounded domain with Lipschitz boundary $\partial\Omega$ and the Dirichlet part Γ_{D} of $\partial\Omega$ is assumed to have positive surface measure. The target manifold $\mathbb{S}^{\ell-1}$ is the unit sphere in $\mathbb{R}^\ell$, which imposes the pointwise constraint $|u(x)| = 1$ a.e. in Ω. We denote by $\nabla u : \Omega \to \mathbb{R}^{d,\ell}$, $(\nabla u)_{ij} = u^i_{x_j}$, the gradient matrix of u, and by $|\cdot|$ both the Euclidean norm on $\mathbb{R}^\ell$ and the Frobenius norm on $\mathbb{R}^{d,\ell}$.

The Euler–Lagrange equations for the Dirichlet energy $I(u)$ are

$$-\Delta u = \lambda u, \quad |u| = 1 \quad \text{in } \Omega, \tag{1.2}$$

$$u = u_{\mathrm{D}} \quad \text{on } \Gamma_{\mathrm{D}}, \quad \frac{\partial u}{\partial n} = 0 \quad \text{on } \partial\Omega \setminus \Gamma_{\mathrm{D}}. \tag{1.3}$$

The function λ is the Lagrange multiplier related to the unit-length constraint and is given by $\lambda = |\nabla u|^2$; see [10, Ch. 7] and references therein.

Such constrained minimization problems are central to various physical models. A natural physical example arises in nematic liquid crystal theory, where the director field describes the average molecular orientation and satisfies the unit-length constraint. Under the one-constant approximation, the Oseen–Frank energy reduces to the Dirichlet energy, and equilibrium configurations correspond exactly to harmonic maps into spheres, [3]. In micromagnetics, the magnetization is likewise modeled by a unit-length vector field, with the Dirichlet energy representing the exchange contribution to the free energy, [29].

Gradient flows provide a natural approach for computing harmonic maps. A prototypical example is the L^2 gradient flow, known as the harmonic map heat flow,

$$u_t - \Delta u = |\nabla u|^2 u, \quad |u| = 1 \quad \text{in } \Omega,$$

with an initial condition $u(\cdot,0) = u^0 \in \mathcal{A}_{u_{\mathrm{D}}}$, Dirichlet boundary conditions $u(\cdot,t)|_{\Gamma_{\mathrm{D}}} = u_{\mathrm{D}}$, and homogeneous Neumann boundary conditions $\partial u/\partial n(\cdot,t) = 0$ on $\Omega \setminus \Gamma_{\mathrm{D}}$, where the class of admissible vector fields $\mathcal{A}_{u_{\mathrm{D}}}$ is defined as

$$\mathcal{A}_{u_{\mathrm{D}}} := \{u \in H^1(\Omega;\mathbb{S}^{\ell-1}) : u|_{\Gamma_{\mathrm{D}}} = u_{\mathrm{D}}\}.$$

Under our assumptions, $\mathcal{A}_{u_{\mathrm{D}}}$ is nonempty. While introduced as a gradient descent method for minimizing the Dirichlet energy, the harmonic map heat flow also captures essential features of dynamical models in physics. The Landau–Lifshitz–Gilbert equation, for instance, augments this flow with damping and precession terms to describe magnetization dynamics, including domain wall motion and vortex formation, [6]. In the theory of nematic liquid crystals, the director evolution in the Ericksen–Leslie model resembles harmonic map heat flow coupled to fluid dynamics through the Navier–Stokes equations, [14, 30]. Similar p.d.e's also arise in the study of mean curvature flow, which governs the evolution of the surface normals; see [27, 28].

The unit-length constraint presents significant challenges for numerical approximation of the harmonic map heat flow, especially in using it to seeking the stationary state. Classical finite element methods and commonly used time-stepping schemes typically produce numerical solutions that do not satisfy the unit-length condition exactly. One straightforward remedy is to apply a projection step as post-processing, which renormalizes the solution by projecting it onto the unit sphere; see [4, 5, 7, 8, 22]. However, renormalization-based methods typically impose restrictions on the time step size to maintain stability and make it difficult to preserve the energy-decay property. A different approach to maintain the unit-length constraint is the use of a Lagrange multiplier, which leads to a saddle-point reformulation of the problem. In this framework, optimal convergence results for piecewise affine finite element discretizations with nodal constraints are established in [12, 13, 26]. An alternative, popular strategy, due to Alouges, [3], is the following weak formulation of the Euler–Lagrange equations (1.2)–(1.3):

seek $u \in \mathcal{A}_{u_D}$ such that

$$(\nabla u, \nabla v) = 0 \quad \forall v \in T_u$$

with

$$T_u := \{v \in \mathcal{H} : v \cdot u = 0 \text{ a.e. in } \Omega\}$$

a *solution-dependent, tangential test space*, a closed subspace of the subspace $\mathcal{H} := H^1_D(\Omega;\mathbb{R}^\ell)$ of $H^1(\Omega;\mathbb{R}^\ell)$ with vanishing traces on $\Gamma_D \subset \partial\Omega$. Such a formulation is amenable to linearization, typically by replacing the unknown u in T_u with an extrapolated approximation. The resulting linear scheme retains the energy-decay property, which is essential for stability.

The idea was also extended to gradient flows in [11], leading to the weak formulation

$$(u_t, v)_\star + (\nabla u, \nabla v) = 0 \quad \forall v \in T_u, \quad t > 0, \tag{1.4}$$

subject to initial and boundary conditions, $u(\cdot,0) = u^0 \in \mathcal{A}_{u_D}$ and $u(\cdot,t)|_{\Gamma_D} = u_D$; the pointwise unit-length constraint is imposed in the equivalent form

$$u_t \cdot u = 0. \tag{1.5}$$

In (1.4), the inner product $(\cdot,\cdot)_\star$ is usually either the L^2 or the H^1 inner product, $(\cdot,\cdot)$ and $(\nabla\cdot,\nabla\cdot)$, respectively, in which cases (1.4) is the L^2 or the H^1 gradient flow for harmonic maps into spheres, respectively. Although these formulations preserve the energy decay property, the linearization process may lead to a violation of the unit-length constraint. In such cases, a projection step, as mentioned previously, can be incorporated to restore the constraint. Nonetheless, these approaches typically necessitate constraints on the time step and mesh acuteness to achieve both the energy decay and the unit-length property; see [9]. It is also worth noting that even stable projections may result in enlarged residual errors in the solution.

These challenges motivated the development of *projection-free methods*. In particular, Bartels [11] initiated a systematic study demonstrating that the projection step can be omitted, leading to constraint violations that decay as the time step size τ decreases. This foundational work introduced a linearly implicit Euler scheme, achieving first-order accuracy of the constraint violation. Building on this idea, subsequent efforts have focused on improving the convergence order of the constraint violation in projection-free schemes, alongside standard objectives such as ensuring energy dissipation and achieving optimal temporal convergence rates. Notably, a second-order *projection-free two-step BDF scheme* was proposed in [1] and a *linearly implicit θ-method* was developed in [2]; the latter accommodates variable time steps and handles nonsmooth initial data. Moreover, for $\theta = 1/2$, the scheme in [2] is a *linearly implicit Crank–Nicolson method* that achieves second-order accuracy in approximating the unit-length constraint. Despite these advances, all existing projection-free methods remain limited to at most second-order accuracy. The construction of higher-order projection-free schemes is still an open challenge—and the central objective of the present work.

To address this challenge, we explore the Gauss family of Runge–Kutta methods as a natural pathway to higher-order projection-free methods. Since the Crank–Nicolson method is the first member of this family, it provides a natural starting point for our generalization. To set the stage, we briefly recall the projection-free Crank–Nicolson schemes introduced in [2]. For a fixed time step τ, and a partition $t_n := n\tau, n = 0,1,\ldots$, the fully implicit Crank–Nicolson method approximates the

orthogonality condition (1.5) at the midpoint $t_{n+1/2} = t_n + \tau/2$ via

$$d_t u^{n+1} \cdot u^{n+1/2} = 0,$$

where the backward difference quotient $d_t u^{n+1} := (u^{n+1} - u^n)/\tau$ approximates the time derivative $u_t(\cdot, t_{n+1/2})$, and $u^{n+1/2} := (u^n + u^{n+1})/2$. The method then seeks $d_t u^{n+1} \in T_{u^{n+1/2}}$ such that

$$(d_t u^{n+1}, \upsilon)_\star + \big(\nabla\big(u^n + \tfrac{1}{2}\tau d_t u^{n+1}\big), \nabla\upsilon\big) = 0 \quad \forall \upsilon \in T_{u^{n+1/2}}. \tag{1.6}$$

The solution at t_{n+1} is approximated via $u^{n+1} := u^n + \tau d_t u^{n+1}$, which respects the Dirichlet boundary condition. This scheme possesses several desirable properties: it dissipates the energy and satisfies the unit-length constraint at the time nodes exactly. However, it is fully implicit, as the tangent space $T_{u^{n+1/2}}$ depends on the yet-unknown u^{n+1}. To facilitate implementation, [2] proposed a *linearly implicit Crank–Nicolson method*, where the constraint is linearized by extrapolating $u^{n+1/2}$ via $\widehat{u}^n := \frac{3}{2}u^n - \frac{1}{2}u^{n-1}$. The increment $d_t u^{n+1} \in T_{\widehat{u}^n}$ is then computed from

$$(d_t u^{n+1}, \upsilon)_\star + \big(\nabla\big(u^n + \tfrac{1}{2}\tau d_t u^{n+1}\big), \nabla\upsilon\big) = 0 \quad \forall \upsilon \in T_{\widehat{u}^n}, \tag{1.7}$$

followed by the same update $u^{n+1} := u^n + \tau d_t u^{n+1}$.

To pave the way for higher-order extensions, it is helpful to reinterpret the Crank–Nicolson method from the perspective of Runge–Kutta methods. Specifically, Crank–Nicolson is the one-stage Gauss method, i.e., the midpoint method, with a single internal node located at the midpoint $t_{n1} := t_n + \tau/2$ of the interval $[t_n, t_{n+1}]$. Then, the increment $\dot{u}^{n1} (= d_t u^{n+1})$ approximates the time derivative $u_t(t_{n1})$, while the internal stage $u^{n1} = u^n + \frac{1}{2}\tau\dot{u}^{n1}$ approximates $u(t_{n1})$; here and in the sequel we abbreviate $u(\cdot, t)$ by $u(t)$. The Crank–Nicolson method can thus be recast in the following form: seek $\dot{u}^{n1} \in T_{u^{n1}}$ such that

$$(\dot{u}^{n1}, \upsilon_1)_\star + \big(\nabla\big(u^n + \tfrac{1}{2}\tau\dot{u}^{n1}\big), \nabla\upsilon_1\big) = 0 \quad \forall \upsilon_1 \in T_{u^{n1}}, \tag{1.8}$$

followed by the update

$$u^{n+1} := u^n + \tau\dot{u}^{n1}. \tag{1.9}$$

This interpretation provides a natural framework for generalization to higher-order Gauss schemes, which constitute our base schemes. The resulting methods, introduced in (2.2)–(2.4), preserve the unit-length constraint, ensure energy decay at the time-discrete level, and achieve high-order accuracy. To enhance practical applicability, we also develop linearizations of the base schemes via a fixed-point iteration strategy, and establish existence and uniqueness of the corresponding approximations. We furthermore prove that the linearized Gauss schemes preserve the energy-decay property. Although the linearized schemes no longer strictly preserve the unit-length constraint, we quantify the constraint violation in terms of the differences between two successive fixed-point iterates. By imposing a threshold on this difference, the linearized schemes maintain the unit-length property up to machine precision. Moreover, even a fixed number of fixed-point iterations significantly improves the convergence order of the constraint violation. Extensive numerical experiments confirm that the linearized variants maintain high-order temporal accuracy as well as high-order convergence in the constraint violation for fixed numbers of iterations. When the stopping criterion is based on the differences between successive iterates, the schemes simultaneously preserve high-order accuracy and the unit-length property within machine precision.

Error analysis is a challenging issue that we leave for future work. In the case of smooth solutions, we expect the order of the q-stage Gauss method to be $q+1$ and $2q$ for the L^2 and H^1 gradient flows, respectively.

The article is organized as follows. In Section 2, we construct and study projection-free Gauss methods with an arbitrary number of stages q, establish their energy decay property and preservation of the unit-length property, and provide an equivalent collocation formulation. In Section 3, we introduce an implementable variant of the fully implicit schemes via fixed-point linearization. Section 4 presents numerical results validating the superiority of the proposed methods.

2. Projection-free Gauss methods

In this section, we extend the Crank–Nicolson (midpoint) method, and devise Gauss methods of arbitrary number of stages q for harmonic maps. These methods have excellent properties for the gradient flow problem (1.4) as they preserve both the unit-length constraint and the energy-decay property; they constitute our base schemes. In the next section, we present an implementable linearization of the base schemes via a fixed-point iteration.

For $q \in \mathbb{N}$, let $0 < c_1 < \cdots < c_q < 1$ denote the Gauss nodes in the interval $(0,1)$. The q-stage Gauss method is specified by the coefficients

$$a_{ij} = \int_0^{c_i} \ell_j(s)\,\mathrm{d}s, \quad b_i = \int_0^1 \ell_i(s)\,\mathrm{d}s, \quad i,j = 1,\dots,q; \tag{2.1}$$

here, $\ell_1,\dots,\ell_q \in \mathbb{P}_{q-1}$ are the Lagrange polynomials for the Gauss nodes $c_1,\dots,c_q$, $\ell_i(c_j) = \delta_{ij}, i,j = 1,\dots,q$. In other words, the *stage order* of the Gauss method is q, whence the method is of collocation type. The first member ($q=1$) of this important family of Runge–Kutta methods is the midpoint (Crank–Nicolson) method.

For a fixed time step τ, and a partition $t_n := n\tau, n = 0,1,\dots$, we denote by $t_{ni} := t_n + c_i\tau, i = 1,\dots,q$, the intermediate nodes. Let $J_n := [t_{n-1}, t_n], n = 1,\dots$, denote the subintervals of the partition.

Let $u^n \in H^1(\Omega;\mathbb{R}^\ell)$ be a given approximation to the nodal value $u(t_n)$ of the solution of (1.4), satisfying the required Dirichlet boundary condition, $u^n|_{\Gamma_\mathrm{D}} = u_\mathrm{D}$. First, in analogy to (1.4), we assign internal *increments* $\dot{u}^{ni} \in T_{u^{ni}}, i = 1,\dots,q$, approximations to the nodal values $u_t(t_{ni})$ of the derivative u_t of u, to internal stages $u^{ni} \in H^1(\Omega;\mathbb{R}^\ell)$, approximations to the nodal values $u(t_{ni})$, by

$$\big(\dot{u}^{ni}, \upsilon_i\big)_\star + \big(\nabla u^{ni}, \nabla \upsilon_i\big) = 0 \quad \forall \upsilon_i \in T_{u^{ni}},\ i = 1,\dots,q. \tag{2.2}$$

Then, we employ the q-stage Gauss method to express the internal stages $u^{ni} \in H^1(\Omega;\mathbb{R}^\ell)$ as well as the next nodal approximation $u^{n+1} \in H^1(\Omega;\mathbb{R}^\ell)$ in terms of the internal increments in the form

$$u^{ni} = u^n + \tau \sum_{j=1}^{q} a_{ij}\dot{u}^{nj}, \quad i = 1,\dots,q, \tag{2.3}$$

and

$$u^{n+1} := u^n + \tau \sum_{i=1}^{q} b_i \dot{u}^{ni}. \tag{2.4}$$

Since $\dot{u}^{ni} \in \mathcal{H}, i = 1,\dots,q$, and u^n satisfies the required Dirichlet boundary condition, it follows immediately from (2.3) and (2.4) that the internal stages u^{ni} and the new approximation u^{n+1} satisfy the Dirichlet boundary condition as well, $u^{ni}|_{\Gamma_\mathrm{D}} = u^{n+1}|_{\Gamma_\mathrm{D}} = u_\mathrm{D}$.

In view of (2.3), (2.2) can be reformulated in the form: seek $\dot{u}^{ni} \in T_{u^{ni}}$ such that

$$(\dot{u}^{ni}, v_i)_\star + \Big(\nabla u^n + \tau \sum_{j=1}^{q} a_{ij} \nabla \dot{u}^{nj}, \nabla v_i\Big) = 0 \quad \forall v_i \in T_{u^{ni}}, \;\; i = 1, \dots, q. \tag{2.5}$$

In the case $q = 1$, (2.5) reduces to the Crank–Nicolson (midpoint) method as given in (1.8).

Furthermore, solving (2.3) for the internal increments $\dot{u}^{ni}$ and substituting the result in the first term in (2.2) as well as in (2.4), we can express the Gauss method in terms of the internal stages u^{ni} and the nodal approximation u^n.

Remark 2.1 (Discrete orthogonality conditions) In our base scheme (2.2)–(2.4), we discretized the unit-length constraint (1.5) componentwise as $\dot{u}^{ni} \in T_{u^{ni}}, i = 1, \dots, q$, i.e.,

$$\dot{u}^{ni} \cdot u^{ni} = 0, \quad i = 1, \dots, q. \tag{2.6}$$

A milder, discrete ℓ^2 orthogonality condition, namely,

$$\sum_{i=1}^{q} b_i \dot{u}^{ni} \cdot u^{ni} = 0, \tag{2.7}$$

is actually sufficient and necessary for the constraint to be satisfied exactly at the nodes, $|u^{n+1}| = |u^n|$; cf. (2.11). See (2.11) as well as (2.25)–(2.26) for the motivation of (2.7).

2.1. *Unit-length and energy-decay properties*

We recall that the Gauss method (2.1) is algebraically stable, that is, the weights $b_1, \dots, b_q$ are nonnegative and the symmetric matrix $M = (m_{ij}) \in \mathbb{R}^{q,q}$ with entries $m_{ij} := b_i a_{ij} + b_j a_{ji} - b_i b_j, i, j = 1, \dots, q$, is positive semidefinite. Actually, the weights $b_1, \dots, b_q$ are positive and M is the zero matrix; see, for instance, [21, Theorem 4.6.1]. The fundamental algebraic stability concept was independently introduced in [15] and [19], and the property $M = 0$ for the Gauss methods was established there as well; see also [16] for earlier related important work on B-stability.

The Gauss methods satisfy the energy-decay as well as the unit-length property; the algebraic stability ensures the former property while the additional fact that $M = 0$ is crucial for the latter property. The unit-length preservation of Gauss methods in the present context of a nonlinear p.d.e. may be viewed as an extension of analogous results by Cooper, [18], concerning the preservation of quadratic invariants for systems of o.d.e's; Runge–Kutta methods with $M = 0$ are called *orbitally stable* in [18].

Proposition 2.1 (unit-length property) *If u^{n+1} satisfies (2.2)–(2.4), then we have*

$$|u^{n+1}| = |u^n|. \tag{2.8}$$

Proof We begin by taking the Euclidean inner product of (2.3) with $\dot{u}^{ni}$, which yields

$$\dot{u}^{ni} \cdot u^{ni} = u^n \cdot \dot{u}^{ni} + \tau \sum_{j=1}^{q} a_{ij} \dot{u}^{ni} \cdot \dot{u}^{nj}, \quad i = 1, \dots, q. \tag{2.9}$$

Taking the squares of the Euclidean norms of both sides of (2.4), we get

$$|u^{n+1}|^2 = |u^n|^2 + 2\tau \sum_{i=1}^{q} b_i u^n \cdot \dot{u}^{ni} + \tau^2 \sum_{i,j=1}^{q} b_i b_j \dot{u}^{ni} \cdot \dot{u}^{nj}, \tag{2.10}$$

and thus, substituting $u^n \cdot \dot{u}^{ni}$ by the expression given in (2.9),

$$|u^{n+1}|^2 = |u^n|^2 + 2\tau \sum_{i=1}^{q} b_i \dot{u}^{ni} \cdot u^{ni} - 2\tau^2 \sum_{i,j=1}^{q} b_i a_{ij} \dot{u}^{ni} \cdot \dot{u}^{nj} + \tau^2 \sum_{i,j=1}^{q} b_i b_j \dot{u}^{ni} \cdot \dot{u}^{nj},$$

i.e.,

$$|u^{n+1}|^2 = |u^n|^2 + 2\tau \sum_{i=1}^{q} b_i \dot{u}^{ni} \cdot u^{ni} - \tau^2 \sum_{i,j=1}^{q} m_{ij} \dot{u}^{ni} \cdot \dot{u}^{nj},$$

whence, in view of $M = 0$,

$$|u^{n+1}|^2 = |u^n|^2 + 2\tau \sum_{i=1}^{q} b_i \dot{u}^{ni} \cdot u^{ni}. \tag{2.11}$$

In particular, in the case of our base scheme (2.2)–(2.4), due to the discrete orthogonality condition (2.6), the second term on the right-hand side of (2.11) vanishes, and we see that the Gauss method satisfies the constraint at the nodes exactly, $|u^{n+1}| = |u^n|$; obviously, the discrete ℓ^2 orthogonality condition (2.7) is sufficient and necessary for this property. □

Next, we turn to proving the energy-decay property of the scheme (2.5), (2.3), (2.4). Since this property also holds for the linearized variant discussed in the next section—where the spaces $T_{u^{ni}}$ are approximated by linearized versions—it is convenient to present the energy-decay argument in a more general setting to avoid repetitions. Specifically, we replace the trial and test spaces $T_{u^{ni}}$ by $T_{w^{ni}}$ with arbitrary vector fields $w^{ni} \in H^1(\Omega;\mathbb{R}^\ell), i = 1,\dots,q$, satisfying the Dirichlet boundary condition, that is, we seek internal increments $\dot{u}^{ni} \in T_{w^{ni}}, i = 1,\dots,q$, such that

$$(\dot{u}^{ni}, \upsilon_i)_\star + \Big(\nabla u^n + \tau \sum_{j=1}^{q} a_{ij} \nabla \dot{u}^{nj}, \nabla \upsilon_i\Big) = 0 \quad \forall \upsilon_i \in T_{w^{ni}}, \;\; i = 1,\dots,q, \tag{2.12}$$

and define the internal stages u^{ni} and the next nodal approximation u^{n+1} by

$$u^{ni} = u^n + \tau \sum_{j=1}^{q} a_{ij} \dot{u}^{nj}, \quad i = 1,\dots,q, \tag{2.13}$$

and

$$u^{n+1} := u^n + \tau \sum_{i=1}^{q} b_i \dot{u}^{ni}. \tag{2.14}$$

Existence and uniqueness of solutions of the linear system of equations (2.12) are established in section 3.1.

Proposition 2.2 (energy decay) *If u^{n+1} satisfies (2.12)–(2.14), then we have*

$$\|\nabla u^{n+1}\|^2 - \|\nabla u^n\|^2 = -2\tau \sum_{i=1}^{q} b_i \|\dot{u}^{ni}\|_\star^2 \leqslant 0. \tag{2.15}$$

Proof First, for the admissible test functions $\upsilon_i = \dot{u}^{ni}$, from (2.12) we obtain

$$\|\dot{u}^{ni}\|_\star^2 + (\nabla u^n, \nabla \dot{u}^{ni}) + \tau \sum_{j=1}^{q} a_{ij} (\nabla \dot{u}^{nj}, \nabla \dot{u}^{ni}) = 0, \quad i = 1, \dots, q. \tag{2.16}$$

Second, taking gradients in (2.14) and subsequently the squares of the L^2-norms of both sides, we get

$$\|\nabla u^{n+1}\|^2 = \|\nabla u^n\|^2 + 2\tau \sum_{i=1}^{q} b_i (\nabla u^n, \nabla \dot{u}^{ni}) + \tau^2 \sum_{i,j=1}^{q} b_i b_j (\nabla \dot{u}^{ni}, \nabla \dot{u}^{nj}),$$

and thus, substituting $(\nabla u^n, \nabla \dot{u}^{ni})$ by the expression given in (2.16),

$$2\tau \sum_{i=1}^{q} b_i \|\dot{u}^{ni}\|_\star^2 + \|\nabla u^{n+1}\|^2 = \|\nabla u^n\|^2 - 2\tau^2 \sum_{i,j=1}^{q} b_i a_{ij} (\nabla \dot{u}^{ni}, \nabla \dot{u}^{nj}) + \tau^2 \sum_{i,j=1}^{q} b_i b_j (\nabla \dot{u}^{ni}, \nabla \dot{u}^{nj}),$$

i.e.,

$$2\tau \sum_{i=1}^{q} b_i \|\dot{u}^{ni}\|_\star^2 + \|\nabla u^{n+1}\|^2 = \|\nabla u^n\|^2 - \tau^2 \sum_{i,j=1}^{q} m_{ij} (\nabla \dot{u}^{ni}, \nabla \dot{u}^{nj}). \tag{2.17}$$

The second term on the right-hand side vanishes since $M = 0$, and we obtain the energy-decay property (2.15), for the general method (2.12)–(2.14). □

2.2. *Equivalent formulation of Gauss methods in collocation form*

Since the stage order of the q-stage Gauss method is q, the method can be equivalently written in collocation form. Here, we give the step of the method in the subinterval $J_{n+1} = [t_n, t_{n+1}]$.

The collocation solution U is a polynomial of degree at most q in t in J_{n+1}. Let us denote by $u^n = U(t_n)$ the already available value of U at the left endpoint t_n of J_{n+1}.

In analogy to the Runge–Kutta formulation, where we first determined the internal increments, that is, discrete time derivatives, and subsequently obtained the internal stages and the nodal approximations, we first determine the time derivative $\dot{U}, \dot{U}(t) \in \mathcal{H}$ for every $t \in J_{n+1}$, of the collocation approximation and subsequently the collocation approximation U itself from the relation

$$U(t) = u^n + \int_{t_n}^{t} \dot{U}(s)\, \mathrm{d}s, \quad t \in [t_n, t_{n+1}]. \tag{2.18}$$

Since $\dot{U}(s) \in \mathcal{H}$, for every $s \in J_{n+1}$, it is obvious that $U(t)$ satisfies the Dirichlet boundary condition $U(t)|_{\Gamma_\mathrm{D}} = u_\mathrm{D}$ if and only if the nodal approximation $u^n = U(t_n)$ satisfies it, $u^n|_{\Gamma_\mathrm{D}} = u_\mathrm{D}$.

The collocation method reads: Seek $\dot{U} : J_{n+1} \to \mathcal{H}, \dot{U} \in \mathbb{P}_{\mathcal{H},n}(q-1)$, such that

$$\big(\dot{U}(t_{ni}), \upsilon_i\big)_\star + \Big(\nabla\Big(u^n + \int_{t_n}^{t_{ni}} \dot{U}(s)\,\mathrm{d}s\Big), \nabla\upsilon_i\Big) = 0 \quad \forall \upsilon_i \in T_{U(t_{ni})}, \quad i = 1,\dots,q. \tag{2.19}$$

The trial space $\mathbb{P}_{\mathcal{H},n}(q-1)$ as well as the various test spaces $T_{U(t_{ni})}$ in (2.19) depend on the internal values $U(t_{ni}), i = 1,\dots,q$, of the numerical solution,

$$\mathbb{P}_{\mathcal{H},n}(q-1) := \Big\{ p(t) = \sum_{i=1}^{q} \ell_{ni}(t) w_i,\ w_i \in T_{U(t_{ni})},\ i = 1,\dots,q \Big\}, \tag{2.20}$$

with $\ell_{ni} \in \mathbb{P}_{q-1}$ the Lagrange polynomials ℓ_i for the nodes $c_1,\dots,c_q$ shifted to the subinterval $J_{n+1} = [t_n, t_{n+1}]$, $\ell_{ni}(t_{nj}) = \delta_{ij}, i, j = 1,\dots,q$.

In view of (2.18), in terms of both $\dot{U}$ and U, the collocation equations (2.19) can be reformulated in a more familiar form as

$$\big(\dot{U}(t_{ni}), \upsilon_i\big)_\star + \big(\nabla U(t_{ni}), \nabla\upsilon_i\big) = 0 \quad \forall \upsilon_i \in T_{U(t_{ni})},\ i = 1,\dots,q. \tag{2.21}$$

Methods (2.2)–(2.4) and (2.19), (2.18) are equivalent in the sense that

$$\dot{U}(t_{ni}) = \dot{u}^{ni}, \quad U(t_{ni}) = u^{ni}, \quad i = 1,\dots,q, \quad \text{and} \quad U(t_{n+1}) = u^{n+1}. \tag{2.22}$$

The proof of this equivalence is an adaptation of the standard proof of the equivalence of collocation methods with q distinct nodes and q-stage Runge–Kutta methods of stage order q; see [23, 33] as well as [24, §II.7, Theorems 7.7 and 7.8]. We do not present the details here for the sake of brevity.

We next present the proofs of the unit-length and energy-decay properties in the framework of collocation methods. We adapt the argument in [32] for the B-stability property of Gauss methods, which is based on their reformulation as collocation methods.

Proposition 2.3 (unit-length and energy-decay properties) *Let U satisfy (2.18)–(2.19). We have the following identity unconditionally,*

$$|U(t_{n+1})| = |U(t_n)|, \tag{2.23}$$

as well as the energy-decay property

$$\|\nabla U(t_{n+1})\|^2 - \|\nabla U(t_n)\|^2 = -2\int_{t_n}^{t_{n+1}} \|\dot{U}(t)\|_\star^2\,\mathrm{d}t \leqslant 0. \tag{2.24}$$

Proof To prove (2.23), we apply the fundamental theorem of calculus to derive

$$|U(t_{n+1})|^2 = |U(t_n)|^2 + \int_{t_n}^{t_{n+1}} \frac{\mathrm{d}}{\mathrm{d}t}|U(t)|^2\,\mathrm{d}t,$$

that is

$$|U(t_{n+1})|^2 = |U(t_n)|^2 + 2\int_{t_n}^{t_{n+1}} \dot{U}(t)\cdot U(t)\,\mathrm{d}t. \tag{2.25}$$

Consequently, a necessary and sufficient condition for (2.23) is the L^2-orthogonality

$$\int_{t_n}^{t_{n+1}} \dot{U}(t)\cdot U(t)\,\mathrm{d}t = 0; \tag{2.26}$$

cf. (2.7). Since the integrand $\dot{U}\cdot U$ in (2.26) is a scalar polynomial of degree at most $2q-1$ in the interval $[t_n, t_{n+1}]$, it is integrated exactly by the Gauss quadrature rule with nodes $t_{n1},\dots,t_{nq}$ and weights

$b_1\tau,\dots,b_q\tau$. Therefore, (2.25) yields, in view of the discrete orthogonality condition $\dot U(t_{ni})\in T_{U(t_{ni})}$,

$$|U(t_{n+1})|^2-|U(t_n)|^2=2\tau\sum_{i=1}^q b_i\dot U(t_{ni})\cdot U(t_{ni})=0. \tag{2.27}$$

To prove (2.24), we choose the admissible test functions $\upsilon_i=\dot U(t_{ni})$ in (2.21) to obtain

$$\|\dot U(t_{ni})\|_\star^2+\big(\nabla U(t_{ni}),\nabla\dot U(t_{ni})\big)=0,\quad i=1,\dots,q. \tag{2.28}$$

Furthermore, in analogy to (2.25), we have

$$\|\nabla U(t_{n+1})\|^2-\|\nabla U(t_n)\|^2=2\int_{t_n}^{t_{n+1}}(\nabla\dot U(t),\nabla U(t))\,\mathrm{d}t.$$

Similarly, since the integrand $(\nabla\dot U,\nabla U)$ is also a scalar polynomial of degree at most $2q-1$ in $[t_n,t_{n+1}]$, we see that

$$\|\nabla U(t_{n+1})\|^2-\|\nabla U(t_n)\|^2=2\tau\sum_{i=1}^q b_i\big(\nabla\dot U(t_{ni}),\nabla U(t_{ni})\big),$$

and thus, in view of (2.28),

$$\|\nabla U(t_{n+1})\|^2-\|\nabla U(t_n)\|^2=-2\tau\sum_{i=1}^q b_i\|\dot U(t_{ni})\|_\star^2; \tag{2.29}$$

cf. (2.15). Now, the positivity of the weights b_i yields the desired energy-decay property of the method, $\|\nabla U(t_{n+1})\|\leqslant\|\nabla U(t_n)\|$. Actually, the energy decay can be quantified: Since $\|\dot U(\cdot)\|_\star^2$, as a polynomial of degree at most $2q-2$ in the interval $[t_n,t_{n+1}]$, is integrated exactly by the Gauss rule, (2.29) can be written in the form

$$2\int_{t_n}^{t_{n+1}}\|\dot U(t)\|_\star^2\,\mathrm{d}t+\|\nabla U(t_{n+1})\|^2=\|\nabla U(t_n)\|^2; \tag{2.30}$$

cf. (2.15). Summation over n yields

$$2\int_0^{t_{n+1}}\|\dot U(t)\|_\star^2\,\mathrm{d}t+\|\nabla U(t_{n+1})\|^2=\|\nabla U(0)\|^2, \tag{2.31}$$

that is, the desired result. □

3. Linearization of the base scheme via fixed-point iteration

The base schemes, the Gauss methods (2.5), (2.3), (2.4), have excellent properties for the gradient flow problem (1.4) as they are energy-decaying and satisfy the unit-length constraint at the time nodes t_n exactly. Their drawback lies in the fact that the base scheme cannot be implemented in this form since it is fully implicit; indeed, the trial and test spaces $T_{u^{ni}}, i=1,\dots,q$, in which the internal increments $\dot u^{ni}$ are sought and to which the test functions υ_i belong, depend on the unknown internal stages u^{ni}. Here, we discuss an implementable fixed-point linearization of the base scheme.

In practice, the number of fixed-point iterations is determined by suitable stopping criteria and varies from time level to time level. Here, to simplify the notation, we consider a fixed number $m\in\mathbb{N}$

of iterations at every time level, with the extension for m depending on n being obvious. We denote by $u_m^n \in H^1(\Omega;\mathbb{R}^\ell)$ the approximations to the nodal values $u(t_n)$. In particular, let $u_m^0 := u^0$ be the starting value.

For given nodal approximation $u_m^n \in H^1(\Omega;\mathbb{R}^\ell)$ as well as starting internal stages $u_0^{ni}, i = 1,\dots,q$, satisfying the Dirichlet boundary condition, we consider the following fixed-point linearization of the base scheme (2.5), (2.3), (2.4): For $\ell = 1,\dots,m$, seek $\dot{u}_\ell^{ni} \in T_{u_{\ell-1}^{ni}}, i = 1,\dots,q$, such that

$$(\dot{u}_\ell^{ni}, \upsilon_i)_\star + \Big(\nabla u_m^n + \tau \sum_{j=1}^{q} a_{ij} \nabla \dot{u}_\ell^{nj}, \nabla \upsilon_i\Big) = 0 \quad \forall \upsilon_i \in T_{u_{\ell-1}^{ni}}, \quad i = 1,\dots,q; \tag{3.1}$$

subsequently, update the internal stages $u_\ell^{ni} \in H^1(\Omega;\mathbb{R}^\ell), i = 1,\dots,q$, by

$$u_\ell^{ni} = u_m^n + \tau \sum_{j=1}^{q} a_{ij} \dot{u}_\ell^{nj}, \quad i = 1,\dots,q. \tag{3.2}$$

The next nodal approximation, $u_m^{n+1} \in H^1(\Omega;\mathbb{R}^\ell)$, is then defined by

$$u_m^{n+1} := u_m^n + \tau \sum_{i=1}^{q} b_i \dot{u}_m^{ni}. \tag{3.3}$$

Notice that all approximations u_ℓ^{ni} and u_m^{n+1} satisfy the Dirichlet boundary condition.

The scheme (3.1)–(3.3) is *linear*, since the trial and test spaces $T_{u_{\ell-1}^{ni}}, i = 1,\dots,q$, are available.

Remark 3.1 (An alternative linearization) Our linearization (3.1)–(3.3) is based on (2.5). An alternative linearization, based on (2.2), is as follows: For $\ell = 1,\dots,m$, seek $\dot{u}_\ell^{ni} \in T_{u_{\ell-1}^{ni}}$ such that

$$(\dot{u}_\ell^{ni}, \upsilon_i)_\star + \big(\nabla u_{\ell-1}^{ni}, \nabla \upsilon_i\big) = 0 \quad \forall \upsilon_i \in T_{u_{\ell-1}^{ni}}, \quad i = 1,\dots,q, \tag{3.4}$$

and update the internal stages $u_\ell^{ni} \in H^1(\Omega;\mathbb{R}^\ell), i = 1,\dots,q$, by (3.2); notice that the previous updates $\dot{u}_{\ell-1}^{ni}$ are used in the second, linear and stiff term in (3.4). Then, define the next nodal approximation, $u_m^{n+1} \in H^1(\Omega;\mathbb{R}^\ell)$, by (3.3). A computational advantage of this linearization is that we need to solve q linear equations of the form (3.4) instead of a system of q linear equations of the form (3.1). A drawback of the alternative linearization is that it does not preserve the energy-decay property. For instance, for $q = 1$,

$$\|\nabla u_m^{n+1}\|^2 = \|\nabla u_m^n\|^2 - 2\tau \|\nabla \dot{u}_m^{n1}\|^2 + \tau^2 \big(\nabla \dot{u}_m^{n1}, \nabla(\dot{u}_m^{n1} - \dot{u}_{m-1}^{n1})\big)$$

and we have no control on the sign of the last term on the right-hand side. Let us also note that if we replace the current updates $\dot{u}_\ell^{nj}$ of the increments in the second term of (3.1) by the available increments $\dot{u}_{\ell-1}^{nj}$, then (3.1) reduces to (3.4).

Remark 3.2 (Initialization of the iterative procedure) One option to initialize the iterative procedure at every time level is the following. Let $I_n U$ be a polynomial of degree at most $\min(q,n)$ in time

interpolating the already available nodal approximations (t_{n-i}, u_m^{n-i}), $i = 0, \dots, \min(q,n)$. Then, we define starting internal stages u_0^{ni} for the iterative procedure (3.1)–(3.2) via extrapolation by

$$u_0^{ni} := (I_n U)(t_{ni}), \quad i = 1, \dots, q. \tag{3.5}$$

For small $n, n < q$, the starting stages u_0^{ni} will be less accurate since we do not have enough data at our disposal; in particular, for $n = 0$, the starting stages $u_0^{0i} = u^0$ are first-order approximations to $u(t_{0i})$. In these subintervals, to compensate for the less accurate starting stages, we may increase the number of iterations, for instance by $q - n$; that is, in case we shall use m iterations, say, for $n \geqslant q$, we could use $m + q - n$ iterations for $n < q$.

For $q = 1$, that is, for the Crank–Nicolson method, we have $u_0^{01} = u^0$ and $u_0^{n1} = \frac{3}{2}u_m^n - \frac{1}{2}u_m^{n-1}$ for $n \geqslant 1$; compare to the extrapolated value $\widehat{u}^n = \frac{3}{2}u^n - \frac{1}{2}u^{n-1}$ entering into the linearly implicit Crank–Nicolson method (1.7).

Alternatively, for $n \geqslant 1$, with $\tilde{I}_n U$ a polynomial of degree at most q in time interpolating $(t_{n-1,i}, u_m^{n-1,i})$, $i = 1, \dots, q$, and (t_n, u_m^n), that is, the final internal stages in the preceding subinterval as well as the nodal approximation at t_n, we can define starting internal stages u_0^{ni} by

$$u_0^{ni} := (\tilde{I}_n U)(t_{ni}), \quad i = 1, \dots, q. \tag{3.6}$$

3.1. *Existence and uniqueness*

Here, we prove existence and uniqueness of the increments $\dot{u}_\ell^{ni}, i = 1, \dots, q$, solutions of the fixed-point iteration (3.1). The proof hinges on the following property of the coefficient matrix $\mathcal{A} = (a_{ij})_{i,j=1,\dots,q}$ (cf. [20]) of the Gauss method: There exists a diagonal matrix D with positive diagonal entries such that the matrix $D\mathcal{A}$ is positive definite, i.e., the coefficient matrix $\mathcal{A}$ is positive definite with respect to the inner product $(\cdot,\cdot)_D := (D\cdot,\cdot)$ on $\mathbb{R}^q$, with $(\cdot,\cdot)$ the Euclidean inner product, or, equivalently, the matrix $D^{1/2}\mathcal{A}D^{-1/2}$ is positive definite; see, e.g., [25, §IV.14, Theorem 14.5] or [21, p. 157 and p. 164].

Now, we introduce local notation: Let

$$\widetilde{\mathcal{U}}_{\ell-1}^n := (u_{\ell-1}^{n1}, \dots, u_{\ell-1}^{nq})^\top, \quad \dot{\mathcal{U}}_\ell^n := (\dot{u}_\ell^{n1}, \dots, \dot{u}_\ell^{nq})^\top, \qquad \mathcal{U}_m^n := (u_m^n, \dots, u_m^n)^\top,$$
$$\mathcal{T}_{\widetilde{\mathcal{U}}_{\ell-1}^n} := T_{u_{\ell-1}^{n1}} \times \cdots \times T_{u_{\ell-1}^{nq}}, \quad \mathcal{V} := (v_1, \dots, v_q)^\top \in \mathcal{T}_{\widetilde{\mathcal{U}}_{\ell-1}^n}.$$

With this notation, denoting by $(\cdot,\cdot)_\star$ and $(\cdot,\cdot)$ also the corresponding product inner products, the system of equations (3.1) for the increments takes the form: Seek $\dot{\mathcal{U}}_\ell^n \in \mathcal{T}_{\widetilde{\mathcal{U}}_{\ell-1}^n}$ such that

$$(\dot{\mathcal{U}}_\ell^n, \mathcal{V})_\star + \tau(\mathcal{A}\nabla\dot{\mathcal{U}}_\ell^n, \nabla\mathcal{V}) = -(\nabla\mathcal{U}_m^n, \nabla\mathcal{V}) \quad \forall \mathcal{V} \in \mathcal{T}_{\widetilde{\mathcal{U}}_{\ell-1}^n},$$

i.e.,

$$(D\dot{\mathcal{U}}_\ell^n, \mathcal{V})_\star + \tau(D\mathcal{A}\nabla\dot{\mathcal{U}}_\ell^n, \nabla\mathcal{V}) = -(\nabla D\mathcal{U}_m^n, \nabla\mathcal{V}) \quad \forall \mathcal{V} \in \mathcal{T}_{\widetilde{\mathcal{U}}_{\ell-1}^n}. \tag{3.7}$$

It is now an immediate consequence of the Lax–Milgram Lemma and the closedness of $\mathcal{T}_{\widetilde{\mathcal{U}}_{\ell-1}^n}$ that $\dot{\mathcal{U}}_\ell^n$ is well defined. Indeed, using the positive definiteness of D and $D\mathcal{A}$, it is easily seen that the bilinear

form $a(\cdot,\cdot) : \mathcal{T}_{\widetilde{\mathcal{U}}^n_{\ell-1}} \times \mathcal{T}_{\widetilde{\mathcal{U}}^n_{\ell-1}} \to \mathbb{R}$,

$$a(\mathcal{U},\mathcal{V}) := (D\mathcal{U},\mathcal{V})_\star + \tau(D\mathcal{O}\nabla\mathcal{U},\nabla\mathcal{V}) \quad \forall \mathcal{U},\mathcal{V} \in \mathcal{T}_{\widetilde{\mathcal{U}}^n_{\ell-1}},$$

is both coercive and bounded (we assume that the norm induced by the inner product $(\cdot,\cdot)_\star$ is dominated by the norm induced by the inner product $(\nabla\cdot,\nabla\cdot)$ on $\mathcal{H}$). Furthermore, the linear form $f : \mathcal{T}_{\widetilde{\mathcal{U}}^n_{\ell-1}} \to \mathbb{R}$,

$$f(\mathcal{V}) := -(\nabla D\mathcal{U}^n_m,\nabla\mathcal{V}) \quad \forall \mathcal{V} \in \mathcal{T}_{\widetilde{\mathcal{U}}^n_{\ell-1}},$$

is obviously bounded.

3.2. *Energy decay property and constraint violation*

The linearized schemes satisfy the energy decay property, but the unit-length constraint is not exactly preserved. Instead, we can quantify the constraint violation.

Proposition 3.1 (energy decay and constraint violation) *Let u^{n+1}_m satisfy (3.1)–(3.3). Then, we have the energy-decay property*

$$\|\nabla u^{n+1}_m\|^2 - \|\nabla u^n_m\|^2 = -2\tau \sum_{i=1}^{q} b_i \|\dot{u}^{ni}_m\|^2_\star \leqslant 0. \tag{3.8}$$

Furthermore, assuming $|u^0_m| = 1$, we have the constraint violation relation

$$\big\||u^n_m|^2 - 1\big\|_{L^1(\Omega)} = 2\tau \int_\Omega \Big| \sum_{k=0}^{n-1} \sum_{i=1}^{q} b_i \dot{u}^{ki}_m \cdot (u^{ki}_m - u^{ki}_{m-1}) \Big| \,\mathrm{d}x, \quad n = 1,2,\dots. \tag{3.9}$$

Proof Note that the linearized scheme (3.1)–(3.3) is a special case of (2.12)–(2.14). Therefore, the energy decay estimate (3.8) follows directly from Proposition 2.2.

To prove (3.9), we proceed analogously to the derivation of (2.10)–(2.11), and obtain

$$|u^{k+1}_m|^2 = |u^k_m|^2 + 2\tau \sum_{i=1}^{q} b_i \dot{u}^{ki}_m \cdot u^{ki}_m,$$

and thus, in view of the orthogonality conditions $\dot{u}^{ki}_m \in T_{u^{ki}_{m-1}}$,

$$|u^{k+1}_m|^2 = |u^k_m|^2 + 2\tau \sum_{i=1}^{q} b_i \dot{u}^{ki}_m \cdot (u^{ki}_m - u^{ki}_{m-1}).$$

Summing here over k, from $k = 0$ to $k = n-1$, and using the fact that $|u^0_m| = 1$, we get

$$|u^n_m|^2 - 1 = 2\tau \sum_{k=0}^{n-1} \sum_{i=1}^{q} b_i \dot{u}^{ki}_m \cdot (u^{ki}_m - u^{ki}_{m-1}), \quad n = 1,2,\dots,$$

which immediately leads to the constraint violation relation (3.9). □

Remark 3.3 (Stopping criterion) As indicated by (3.9), the constraint violation is controlled by the difference between two successive iterates of the fixed-point iteration. For sufficiently large m, the right-hand side of (3.9) is expected to become small.

This observation also suggests a natural stopping criterion for the fixed-point iteration: the iteration may be terminated once a suitable norm of the differences $u_m^{ni} - u_{m-1}^{ni}$ falls below a prescribed tolerance.

3.3. *Linearizied Crank–Nicolson method via fixed-point iteration*

For $q = 1$, we have $a_{11} = 1/2, b_1 = 1$, and method (3.1)–(3.3), that is, the fixed-point linearization of the Crank–Nicolson method, reads: For $\ell = 1, \dots, m$, seek increments $\dot{u}_\ell^{n1} \in T_{u_{\ell-1}^{n1}}$ such that

$$(\dot{u}_\ell^{n1}, \upsilon)_\star + \big(\nabla u_m^n + \tfrac{1}{2}\tau\nabla\dot{u}_\ell^{n1}, \nabla\upsilon\big) = 0 \quad \forall \upsilon \in T_{u_{\ell-1}^{n1}}, \tag{3.10}$$

and update both the internal stage $u_\ell^{n1} \in H^1(\Omega;\mathbb{R}^\ell)$ and the nodal approximation $u_\ell^{n+1} \in H^1(\Omega;\mathbb{R}^\ell)$ by

$$u_\ell^{n1} := u_m^n + \frac{1}{2}\tau\dot{u}_\ell^{n1} \tag{3.11}$$

and

$$u_\ell^{n+1} := u_m^n + \tau\dot{u}_\ell^{n1}. \tag{3.12}$$

The internal stages u_ℓ^{n1} and the approximations u_ℓ^{n+1} satisfy the Dirichlet boundary condition. For convenience, we introduced here all updates u_ℓ^{n+1} of the nodal approximation, while in (3.3) we only introduced the final update u_m^{n+1}. As starting values u_0^{n1} for the internal stages in the fixed-point iteration procedure (3.10), following either (3.5) or (3.6), we can use the extrapolated values

$$u_0^{01} := u_m^0 := u^0 \quad \text{and} \quad u_0^{n1} := \frac{3}{2}u_m^n - \frac{1}{2}u_m^{n-1}, \ \ n \geqslant 1.$$

It follows immediately from (3.11) and (3.12) that

$$\dot{u}_\ell^{n1} = \frac{u_\ell^{n+1} - u_m^n}{\tau} =: d_\tau u_\ell^{n+1} \quad \text{and} \quad u_\ell^{n1} = \frac{1}{2}(u_\ell^{n+1} + u_m^n) =: u_\ell^{n+\frac{1}{2}}.$$

Thus, we can rewrite (3.10)–(3.12) in a more familiar form for the Crank–Nicolson method: seek increments $d_t u_\ell^{n+1} \in T_{u_{\ell-1}^{n+\frac{1}{2}}}$ such that

$$(d_t u_\ell^{n+1}, \upsilon)_\star + \big(\nabla\big(u_m^n + \tfrac{1}{2}\tau d_t u_\ell^{n+1}\big), \nabla\upsilon\big) = 0 \quad \forall \upsilon \in T_{u_{\ell-1}^{n+\frac{1}{2}}} \tag{3.13}$$

and update the nodal approximation $u_\ell^{n+1} \in H^1(\Omega;\mathbb{R}^\ell)$ by

$$u_\ell^{n+1} := u_m^n + \tau d_t u_\ell^{n+1}. \tag{3.14}$$

In the fixed-point iteration procedure (3.13)–(3.14), the corresponding starting values u_0^{n+1} for the nodal approximations are the extrapolated values

$$u_0^1 := u_m^0 := u^0 \quad \text{and} \quad u_0^{n+1} := 2u_m^n - u_m^{n-1}, \ \ n \geqslant 1.$$

Constraint violation. Taking the Euclidean inner product with $2u_m^{n+\frac{1}{2}} = u_m^{n+1} + u_m^n$ in the relation $u_m^{n+1} - u_m^n = \tau d_t u_m^{n+1}$, we obtain

$$|u_m^{n+1}|^2 - |u_m^n|^2 = 2\tau d_t u_m^{n+1} \cdot u_m^{n+\frac{1}{2}},$$

and thus, in view of the orthogonality $d_t u_m^{n+1} \cdot u_{m-1}^{n+\frac{1}{2}} = 0$,

$$|u_m^{n+1}|^2 - |u_m^n|^2 = 2\tau d_t u_m^{n+1} \cdot \big(u_m^{n+\frac{1}{2}} - u_{m-1}^{n+\frac{1}{2}}\big),$$

i.e.,

$$|u_m^{n+1}|^2 - |u_m^n|^2 = \tau d_t u_m^{n+1} \cdot (u_m^{n+1} - u_{m-1}^{n+1}),$$

which we can also write in the form

$$|u_m^{n+1}|^2 = |u_m^n|^2 + (u_m^{n+1} - u_m^n) \cdot (u_m^{n+1} - u_{m-1}^{n+1}).$$

4. Numerical examples

In this section, we illustrate and validate the performance of the proposed methods through a series of numerical experiments, focusing on the following key aspects: constraint violation, convergence rates of the errors of the numerical solutions at a fixed final time T, and energy errors. Since (3.1)–(3.3) describe the temporal semi-discretization, we first present implementable algorithms by addressing spatial discretization, the stopping criterion for the fixed-point iteration, and the selection of the starting guesses.

For full discretization, we employ the finite element method for spatial discretization and handle the orthogonality condition required in (3.1) by introducing Lagrange multipliers. Specifically, we consider an unstructured triangular mesh $\mathcal{T}_h$ of Ω and use the first-order H^1-conforming finite elements, i.e., the space $V_h^3 \subset H^1(\Omega;\mathbb{R}^3)$, where V_h consists of continuous, piecewise linear functions. The orthogonality condition in the variational formulation of the method, i.e., $\dot{u}_\ell^{ni} \in T_{u_{\ell-1}^{ni}}$, is enforced only at the vertices of $\mathcal{T}_h$.

To this end, we denote by $\mathcal{I}_h$ the Lagrange interpolation operator onto V_h (or V_h^3). We also introduce the mass-lumped inner product $(\cdot,\cdot)_h$ as

$$(u,v)_h := \int_\Omega \mathcal{I}_h(uv)\,\mathrm{d}x.$$

With this notation, this pointwise orthogonality can be formulated by requiring

$$(\lambda_i \dot{u}_\ell^{ni}, u_{\ell-1}^{ni})_h = 0 \quad \forall \lambda_i \in V_h, \;\; i = 1,\dots,q.$$

We first consider the performance of the linearized Gauss methods, via fixed-point iteration, when seeking stationary states of the Dirichlet energy. To this end, we terminate the fixed-point iteration when the differences of two consecutive increment iterates, $\dot{u}_{\ell-1}^{ni}$ and $\dot{u}_\ell^{ni}$, do not exceed a fixed tolerance $\varepsilon_{\mathrm{Non}} = 10^{-6}$ as elaborated in Remark 3.3; see (4.2). Since each time step may require a different number of iterations before being terminated, we denote this number as m_n for clarity. The fully discretized method is summarized in Algorithm 4.1.

Algorithm 4.1 Linearized Gauss methods

1: **Input:** Choose $u^0 \in V_h^3$ with $u^0|_{\Gamma_D} = (\mathcal{I}_h \tilde{u}_D)|_{\Gamma_D}$ and $\mathcal{I}_h(|u^0|^2) = 1$. Set $n = 0$.
2: **Step 1:**

1.0 Initialization: Set u_0^{ni} as commented in Remark 3.2 for $i = 1, \dots, q$. Set $\ell = 1$.
1.1 For $i = 1, \dots, q$, seek internal increments $\dot{u}_\ell^{ni} \in V_h^3$ and $\mu^i \in V_h$ such that

$$\begin{aligned}(\dot{u}_\ell^{ni}, \upsilon_i)_\star + \Big(\nabla u_{m_n}^n + \tau \sum_{j=1}^q a_{ij} \nabla \dot{u}_\ell^{nj}, \nabla \upsilon_i\Big) \\ + (\lambda_i \dot{u}_\ell^{ni}, u_{\ell-1}^{ni})_h - (\mu^i \upsilon_i, u_{\ell-1}^{ni})_h = 0 \quad \forall \upsilon_i \in V_h^3 \ \ \forall \lambda_i \in V_h.\end{aligned} \tag{4.1}$$

1.2 Check the stopping criterion

$$\|\dot{u}_\ell^{ni} - \dot{u}_{\ell-1}^{ni}\|_\star + \tau \sum_{j=1}^q |a_{ij}| \|\nabla(\dot{u}_\ell^{nj} - \dot{u}_{\ell-1}^{nj})\|_{L^2} \leqslant \varepsilon_{\mathrm{Non}}, \quad i = 1, \dots, q. \tag{4.2}$$

If the stopping criterion is satisfied, set $m_{n+1} = \ell$, and go to **Step 2** with

$$u_{m_{n+1}}^{n+1} = u_{m_n}^n + \tau \sum_{i=1}^q b_i \dot{u}_{m_n}^{ni}. \tag{4.3}$$

Else, increase $\ell \to \ell + 1$ and go to Step 1.1.

3: **Step 2:** Stop if

$$\|\dot{u}_{m_n}^{ni}\|_\star + \tau \sum_{j=1}^q |a_{ij}| \, \|\nabla \dot{u}_{m_n}^{nj}\| \leqslant \varepsilon_{\mathrm{stop}}, \quad i = 1, \dots, q. \tag{4.4}$$

4: **Step 3:** Increase $n \to n + 1$ and go to **Step 1**.

In the following, we present two variants of Algorithm 4.1, each tailored to investigate specific aspects of the proposed method. These variants are implemented by making slight modifications to Algorithm 4.1, with a focus on fixing the final computational time T as well as the number m_0 of iterations. For clarity, we refer to these variants as Algorithm 4.1a and Algorithm 4.1b, and describe them below along with their corresponding modifications.

Fixed computational time T: This variant is designed to study the temporal convergence rates of the proposed linearized Gauss methods for approximating solutions of the gradient flow problem. The modification to Algorithm 4.1 is as follows:

Algorithm 4.1a Linearized Gauss method with a fixed computational time T

1: **Parameter selection:** Choose $\tau = T/N$ for some $N \in \mathbb{N}$.
2: **Modified Step 2:** Stop if $n\tau \geqslant T$.

Algorithm 4.1a allows us to validate the temporal convergence of the method by measuring the differences of numerical solutions of refined time steps as given in (4.11).

Fixed number m_0 of iterations: The second variant focuses on illustrating the performance of the fixed-point linearization (3.1)–(3.2) with a fixed number m_0 of iterations. By fixing the number of

iterations, we can more clearly demonstrate the gain in increasing m_0 and furthermore establish a direct connection to the linearly implicit Crank–Nicolson method devised in [2]. Specifically, for $q = 1$ and $m_0 = 1$, Algorithm 4.1b is almost the same with the linearly implicit Crank–Nicolson method with the only difference consisting in the computation of u^1. To be specific, the linearly implicit Crank–Nicolson method in [2] employs the linearly implicit Euler method in the first step. In contrast, Algorithm 4.1b computes u^1 by performing $m_0 + 1$ iterations with starting internal stage $u_0^{01} = u^0$. The modification to Algorithm 4.1 for this variant, for the initialization (3.6), is as follows:

Algorithm 4.1b Fixed-point linearization with a fixed number m_0 of iterations

1: **Modified Step 1:**

1.2 stops if $\ell = m_0$ for $n \geqslant 1$ or
stops if $\ell = m_0 + q$ for $n = 0$, as suggested in Remark 3.2.
Else, increase $\ell \to \ell + 1$ and go to Step 1.1.

In all computations, we consider the model problem described in [1, Section 4.1]. The domain $\Omega = (-1/2, 1/2)^2$ is discretized using a fixed unstructured triangular mesh generated by Netgen [31]. The mesh consists of 2198 triangles with a mesh size of $h \approx 3.2 \cdot 10^{-2}$. The inverse stereographic projection $\pi_{\mathrm{st}}^{-1} : \Omega \to S^2$ is defined for $\boldsymbol{x} = (x, y) \in \Omega$ as

$$\pi_{\mathrm{st}}^{-1}(\boldsymbol{x}) = \frac{1}{x^2 + y^2 + 1} \begin{pmatrix} 2x \\ 2y \\ 1 - x^2 - y^2 \end{pmatrix}. \tag{4.5}$$

It is well known that the inverse stereographic projection minimizes the Dirichlet energy among all unit-length vector fields satisfying the Dirichlet boundary condition

$$u_{\mathrm{D}} = \pi_{\mathrm{st}}^{-1}|_{\partial\Omega} \quad \text{on } \Gamma_{\mathrm{D}} = \partial\Omega. \tag{4.6}$$

In other words, π_{st}^{-1} is the stationary solution of the gradient flow problem.

4.1. *Convergence test of Algorithm 4.1a*

In this section, we investigate the temporal convergence rate of the proposed method for the gradient flow problem (1.4) with initial value u^0 a perturbation of (4.5), namely,

$$u^0 = \frac{v^0}{|v^0|}, \quad v^0(\boldsymbol{x}) = \frac{1}{x^2 + y^2 + 1} \begin{pmatrix} 2x \\ 2y \\ 1 - x^2 - y^2 \end{pmatrix} + \sin(2\pi x)\sin(2\pi y) \begin{pmatrix} 1 \\ 1 \\ 1 \end{pmatrix}. \tag{4.7}$$

Obviously, u^0 satisfies the Dirichlet boundary condition (4.6). To measure the temporal convergence rate, we consider the approximation error of the solution at some prescribed T, and apply Algorithm 4.1a.

4.1.1. H^1 gradient flow

We begin with testing Algorithm 4.1a for the H^1-gradient flow, considering various numbers of stages, $q = 1, 2, 3$. Since the exact solution at T is unavailable, we compute the errors by comparing the

numerical solutions $u_{h,\tau}$ at time T for consecutively refined step sizes τ, as defined in (4.11). This treatment is similar to using a reference solution with sufficiently small time step size τ. In addition to evaluating the convergence order, we also verify the unit-length property of linearized Gauss methods within machine-precision bounds. The relevant quantities are defined as follows:

1. Constraint violations:

   a. L^1-norm of the constraint violation:

$$\delta_{\mathrm{uni}}[u_{h,\tau}] = \big\|\mathcal{I}_h(|u_{h,\tau}|^2 - 1)\big\|_{L^1}. \tag{4.8}$$

   b. L^∞-norm of the constraint violation:

$$\delta_{\infty}[u_{h,\tau}] = \big\|\mathcal{I}_h(|u_{h,\tau}| - 1)\big\|_{L^\infty}. \tag{4.9}$$

2. Energy differences of numerical solutions of two time step sizes:

$$\delta^{\mathrm{rel}}_{\mathrm{ener}}[u_{h,\tau}] = \big|I(u_{h,\tau}) - I(u_{h,\tau/2})\big|. \tag{4.10}$$

3. L^2 and H^1 approximation errors:

$$L^2\text{-error} = \|u_{h,\tau} - u_{h,\tau/2}\|_{L^2}, \quad H^1\text{-error} = \|u_{h,\tau} - u_{h,\tau/2}\|_{H^1}. \tag{4.11}$$

The convergence rates for the energy error $\delta^{\mathrm{rel}}_{\mathrm{ener}}[u_{h,\tau}]$, the L^2 error, and the H^1 error are denoted by $\mathrm{eoc}^{\mathrm{rel}}_{\mathrm{eng}}$, eoc_{L^2}, and eoc_{H^1}, respectively.

In Algorithm 4.1a, the tolerance in the stopping criterion (4.2) for the iterations at every time level is set to $\varepsilon_{\mathrm{Non}} = 10^{-10}$. The number of fixed-point iterations required to satisfy this threshold at the n-th time step is denoted by m_n, and the maximum number of all iterations across all time steps is defined as $\mathrm{Iter}_{\mathrm{Non}} := \max_{n\geqslant 1} m_n$.

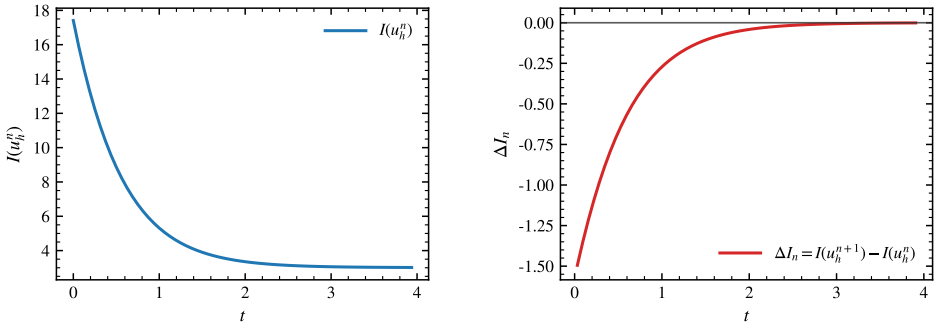

FIG. 4.1. Performance of the linearized Gauss methods for the H^1 gradient flow in $[0,4]$ with $\tau = 2^{-4}$: Evolution of the energy $I(u_h^n)$ (left); energy change $\Delta I_n = I(u_h^{n+1}) - I(u_h^n)$ (right). Experiment of Section 4.1.1.

In this experiment, we test the performance of the linearized q-stage Gauss methods, $q = 1,2,3$, by choosing the time step sizes as $\tau = 2^0, \ldots, 2^{-4}$. The numerical results are presented in Table 4.1. As shown in the last column of Table 4.1, the number of iterations for all cases does not exceed 10.

τ	$\delta_\infty[u_{h,\tau}]$	$\delta_{\text{uni}}[u_{h,\tau}]$	$\delta^{\text{rel}}_{\text{ener}}[u_{h,\tau}]$	$\text{eoc}^{\text{rel}}_{\text{eng}}$	L^2 error	eoc_{L^2}	H_1 error	eoc_{H^1}	Iter_{Non}
1-stage Gauss method									
2^0	3.578e-12	1.327e-12	2.990e-03	–	2.086e-03	–	2.870e-02	–	10
2^{-1}	1.859e-13	5.387e-14	8.826e-04	1.76	5.274e-04	1.98	7.271e-03	1.98	10
2^{-2}	2.549e-13	8.158e-14	2.291e-04	1.95	1.321e-04	2.00	1.822e-03	2.00	9
2^{-3}	1.558e-13	5.067e-14	5.780e-05	1.99	3.304e-05	2.00	4.557e-04	2.00	7
2^{-4}	7.983e-14	2.648e-14	1.448e-05	2.00	8.260e-06	2.00	1.139e-04	2.00	6
2-stage Gauss method									
2^0	2.227e-12	6.852e-13	5.504e-05	–	3.033e-05	–	4.454e-04	–	8
2^{-1}	4.891e-13	1.260e-13	3.235e-06	4.09	1.789e-06	4.08	2.630e-05	4.08	8
2^{-2}	2.147e-13	8.559e-14	1.991e-07	4.02	1.101e-07	4.02	1.620e-06	4.02	7
2^{-3}	3.886e-14	3.096e-14	1.239e-08	4.01	6.857e-09	4.01	1.009e-07	4.01	6
2^{-4}	3.819e-14	6.042e-14	7.736e-10	4.00	4.282e-10	4.00	6.298e-09	4.00	5
3-stage Gauss method									
2^0	2.196e-13	6.562e-14	4.002e-07	–	2.223e-07	–	3.204e-06	–	8
2^{-1}	3.670e-13	1.225e-13	6.486e-09	5.95	3.639e-09	5.93	5.165e-08	5.95	7
2^{-2}	5.762e-14	2.453e-14	1.027e-10	5.98	5.782e-11	5.98	8.166e-10	5.98	6
2^{-3}	3.308e-14	1.381e-14	1.650e-12	5.96	9.178e-13	5.98	1.287e-11	5.99	5
2^{-4}	5.418e-14	2.022e-14	4.530e-14	5.19	1.761e-14	5.70	3.902e-13	5.04	4

TABLE 4.1 *Performance of linearized Gauss methods: H^1 gradient flow at $T = 4$. Experiment of Section 4.1.1.*

Furthermore, the number of iterations decreases with decreasing time step size or increasing number of stages q. This behavior indicates that the computational cost of the linearization via fixed-point iteration remains relatively low, making higher-order methods increasingly competitive. In return, for this modest computational cost, the numerical solution satisfies the unit-length property up to machine precision for $q = 1, 2, 3$, in agreement with the theoretical result derived in (2.23).

Furthermore, for the linearized q-stage Gauss method, Table 4.1 demonstrates that the L^2, H^1, and energy errors at $T = 4$ exhibit a convergence order of $2q$. These results confirm that the method achieves the optimal convergence order of the q-stage Gauss method.

In addition, Figure 4.1 depicts the evolution of the Dirichlet energy $I(u_h^n)$ of the numerical solution at t_n, together with its step-to-step change $\Delta I_n := I(u_h^{n+1}) - I(u_h^n)$, computed with the time step $\tau = 2^{-4}$ and $q = 1$. The results validate the energy decay property stated in Proposition 3.1.

4.1.2. L^2 gradient flow

Next, we repeat this convergence test for the L^2-gradient flow, focusing on a smaller final computation time, $T = 2^{-4}$, and time step sizes $\tau = 2^{-9}, \ldots, 2^{-13}$. The results for $q = 1, 2, 3$ stages are summarized in Table 4.2. Similar to the results for the H^1-gradient flow, no more than 10 iterations are required and the numerical solutions of the L^2-gradient flow also satisfy the unit-length property up to machine precision for $q = 1, 2, 3$. For $q = 1$, we observe a second-order temporal convergence rate for the H^1, L^2, and energy errors. For $q = 2, 3$, the numerical results do not exhibit clear evidence of order of convergence $2q$; this behavior can be attributed to the well-known order reduction phenomenon for high order Runge–Kutta methods.

τ	$\delta_\infty[u_{h,\tau}]$	$\delta_{\text{uni}}[u_{h,\tau}]$	$\delta^{\text{rel}}_{\text{ener}}[u_{h,\tau}]$	$\text{eoc}^{\text{rel}}_{\text{eng}}$	L^2 error	eoc_{L^2}	H_1 error	eoc_{H^1}	Iter_{Non}
1-stage Gauss method									
2^{-9}	8.238e-14	7.671e-15	2.254e-07	–	1.987e-05	–	1.327e-03	–	9
2^{-10}	1.821e-14	2.503e-15	1.652e-07	0.45	4.376e-06	2.18	3.184e-05	5.38	9
2^{-11}	9.770e-15	1.528e-15	4.180e-08	1.98	1.091e-06	2.00	7.940e-06	2.00	9
2^{-12}	7.438e-15	1.343e-15	1.050e-08	1.99	2.725e-07	2.00	1.983e-06	2.00	8
2^{-13}	5.107e-15	1.570e-15	2.627e-09	2.00	6.812e-08	2.00	4.958e-07	2.00	8
2-stage Gauss method									
2^{-9}	7.283e-14	2.989e-14	6.085e-08	–	7.279e-07	–	6.888e-06	–	9
2^{-10}	3.797e-14	5.946e-14	4.203e-09	3.86	5.945e-08	3.61	4.191e-07	4.04	8
2^{-11}	7.172e-14	1.207e-13	2.945e-10	3.83	5.122e-09	3.54	3.398e-08	3.62	8
2^{-12}	1.412e-13	2.423e-13	1.619e-11	4.18	5.711e-10	3.16	3.265e-09	3.38	8
2^{-13}	2.889e-13	4.868e-13	7.199e-13	4.49	6.014e-11	3.25	3.188e-10	3.36	7
3-stage Gauss method									
2^{-9}	1.288e-14	5.323e-15	8.460e-10	–	3.628e-08	–	2.422e-07	–	8
2^{-10}	2.376e-14	1.044e-14	6.842e-11	3.63	3.783e-09	3.26	2.109e-08	3.52	8
2^{-11}	4.752e-14	2.246e-14	2.838e-12	4.59	6.465e-10	2.55	3.260e-09	2.69	8
2^{-12}	9.504e-14	4.608e-14	5.942e-13	2.26	5.678e-11	3.51	2.839e-10	3.52	7
2^{-13}	1.901e-13	9.301e-14	1.781e-13	1.74	2.276e-12	4.64	1.145e-11	4.63	7

TABLE 4.2 *Performance of linearized Gauss methods: L^2 gradient flow at $T = 2^{-4}$. Experiment of Section 4.1.2.*

4.2. *Stationary state of the gradient flow problem*

In this section, we investigate the approximation of the stationary state for the gradient flow problem described in (4.5) using Algorithm 4.1. Compared with the experiment in the preceding section, we again use the initial value of (4.7), but without some prescribed T. Instead, we follow the stopping criterion, defined in (4.4), with tolerance set to $\varepsilon_{\text{stop}} = 10^{-6}$ in the implementation. The total number of time steps required to reach this threshold is denoted by N_{stop}.

In addition to measuring the constraint violation as defined in (4.9), we also evaluate the error between the energy of the numerical solution and that of the stationary state. Due to the use of a coarse mesh in our numerical implementation, the energy error between the numerical solution and the exact stationary solution is typically dominated by spatial discretization errors. To better reflect the impact of the time step size on the energy error, we consider the following quantity, which measures the difference in energy between the numerical solution and the interpolant of the exact solution,

$$\delta_{\text{ener}}[u_{h,\tau}] := \left| I(u_{h,\tau}) - I(\mathcal{I}_h \pi_{\text{st}}^{-1}) \right|. \tag{4.12}$$

The corresponding convergence rate for $\delta_{\text{ener}}[u_{h,\tau}]$ is denoted by eoc_{eng}.

We perform experiments for both the H^1 and L^2 gradient flows using various time step sizes. The results are summarized in Table 4.3. For these cases, we observe that $N_{\text{stop}} \propto \tau^{-1}$. The results further validate that the linearized Gauss methods preserve the unit-length property up to machine precision, while the computational cost remains moderate, as evidenced by the number (no more than 10) of iterations. Notably, for the H^1 gradient flow, even when using the coarsest time step ($\tau = 2^0$), the energy accuracy is comparable to that achieved with the finest time step ($\tau = 2^{-3}$). In contrast, for linearly implicit methods, such as the linearly implicit Crank–Nicolson method discussed in [2], the coarsest

τ	N_{stop}	$\delta_\infty[u_{h,\tau}]$	$\delta_{\text{ener}}[u_{h,\tau}]$	Iter_{Non}
1-stage Gauss method				
2^{0}	17	3.541e-12	3.884e-07	10
2^{-1}	34	2.266e-13	3.884e-07	10
2^{-2}	67	2.716e-13	3.884e-07	9
2^{-3}	133	1.597e-13	3.884e-07	7
2-stage Gauss method				
2^{0}	18	2.230e-12	3.884e-07	8
2^{-1}	35	4.814e-13	3.884e-07	8
2^{-2}	68	1.877e-13	3.884e-07	7
2^{-3}	134	9.592e-14	3.884e-07	6

(a) H^1 gradient flow

τ	N_{stop}	$\delta_\infty[u_{h,\tau}]$	$\delta_{\text{ener}}[u_{h,\tau}]$	Iter_{Non}
1-stage Gauss method				
2^{-9}	179	8.082e-14	2.721e-07	9
2^{-10}	356	2.143e-14	2.721e-07	9
2^{-11}	711	1.210e-14	2.721e-07	9
2^{-12}	1421	1.166e-14	2.721e-07	8
2-stage Gauss method				
2^{-9}	179	1.377e-13	2.721e-07	9
2^{-10}	357	2.112e-13	2.721e-07	8
2^{-11}	712	4.250e-13	2.721e-07	8
2^{-12}	1422	8.360e-13	2.721e-07	8

(b) L^2 gradient flow

TABLE 4.3 *Approximation of stationary solutions by linearized Gauss methods. Experiment of Section 4.2.*

time step results in significantly larger constraint violations, which ultimately lead to substantial energy errors. This underscores the superior performance of Gauss methods linearized via fixed point iteration in Algorithm 4.1.

4.3. *Performance of Algorithm 4.1b with a fixed number m_0 of iterations*

In this section, we investigate the performance of Algorithm 4.1b with a fixed number m_0 of iterations in approximating stationary states of the gradient flow problem.

We primarily investigate the L^1-norm of the constraint violation at the time when the stopping criterion (4.4) is satisfied, with results for $q = 1,2,3$ displayed in Figure 4.2. The corresponding behavior in the L^∞-norm is analogous and therefore omitted. For the H^1 gradient flow, the constraint violation demonstrates a convergence rate of $2q$ for $m_0 = q$. For the L^2 gradient flow, order reduction is observed for $m_0 = q$, similar to the behavior discussed in Section 4.1.2. We emphasize that, for fixed q, even a slight increase of the number m_0 of iterations significantly improves the quality of the approximations regarding the unit-length property.

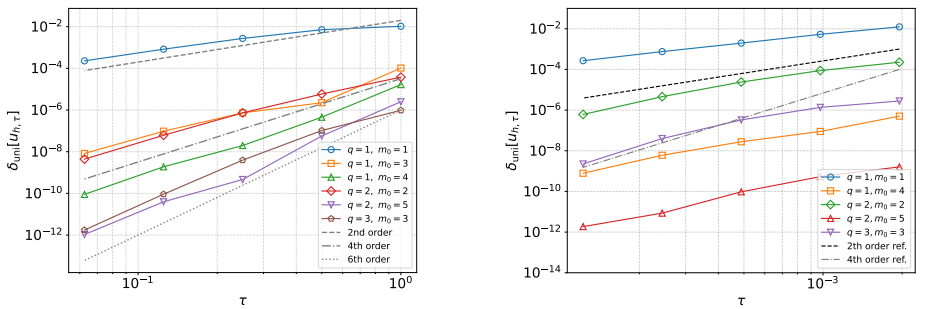

FIG. 4.2. Performance of linearized Gauss methods with fixed m_0: left—H^1 gradient flow; right—L^2 gradient flow (Section 4.3).

τ	N_{stop}	$\delta_\infty[u_{h,\tau}]$	eoc_∞	$\delta_{\text{uni}}[u_{h,\tau}]$	eoc_{uni}	$\delta_{\text{ener}}[u_{h,\tau}]$	eoc_{eng}
$q=1$ & $m_0=1$							
2^0	16	1.861e-02	–	1.045e-02	–	2.900e-02	–
2^{-1}	33	1.424e-02	0.39	7.173e-03	0.54	2.122e-02	0.45
2^{-2}	67	5.586e-03	1.35	2.730e-03	1.39	8.828e-03	1.27
2^{-3}	133	1.717e-03	1.70	8.315e-04	1.72	2.789e-03	1.66
2^{-4}	264	4.746e-04	1.86	2.289e-04	1.86	7.768e-04	1.84

TABLE 4.4 *Performance of the Gauss method for $q=1$ (Crank–Nicolson) linearized via fixed-point iteration with $m_0=1$: H^1 gradient flow. Experiment of Section 4.3.*

Furthermore, we highlight that for $q=1$ and $m_0=1$, Algorithm 4.1b is nearly identical to the linearly implicit Crank–Nicolson method described in [2]. Its performance, as presented in Table 4.4, is also comparable to the results reported in [2, Table 4.1], up to a constant factor arising from differences in the treatment of the first time step.

4.4. *Performance in the presence of singularities*

In this section, we consider a special initial value that leads to a singular solution at an intermediate time (around $T=0.0576$) for the harmonic map heat flow, i.e., the L^2 gradient flow problem. The initial value, taken from [17], is defined as

$$u^0(\boldsymbol{x}) = |\boldsymbol{x}|^{-1} \begin{pmatrix} \sin\varphi(2|\boldsymbol{x}|)\,\boldsymbol{x} \\ |\boldsymbol{x}|\cos\varphi(2|\boldsymbol{x}|) \end{pmatrix}, \tag{4.13}$$

where $\varphi(s)=\frac{3\pi}{2}\min(s^2,1)$. For numerical results of the harmonic map heat flow with this initial value, we refer the reader to [11] and [2] for the linearly implicit Euler and Crank–Nicolson methods, respectively.

In Figure 4.3, we illustrate the numerical solution computed by the linearized one-stage Gauss method for the L^2 gradient flow with $\tau=2^{-12}$. The numerical solutions are vector fields in Ω, visualized by using arrows to indicate the vectors, while the color represents the third component of the vector field, ranging from -1 (blue) to 1 (red). Initially, the vector field is smooth, with vectors pointing upward for points closer to the origin and downward for points near the circle $x^2+y^2=1/6$. As time evolves, the upward-pointing vectors gradually flip downward, and a singularity develops around $T=0.0576$.

In Figure 4.4, we show the evolution of the energy and the constraint violation of the numerical solutions computed by Algorithm 4.1. The results demonstrate that the unit-length property is preserved up to machine precision. Additionally, we observe an abrupt decay in energy around $T=0.0576$, corresponding to the time at which the singularity vanishes.

Funding

This work was partially supported by the National Natural Science Foundation of China (Grant No. 12471371), the Shenzhen Science and Technology Program (Grant No. RCJC20231211090005019), and the Hong Kong Research Grants Council (Projects Nos. 15301321 and RFS2324-5S03).

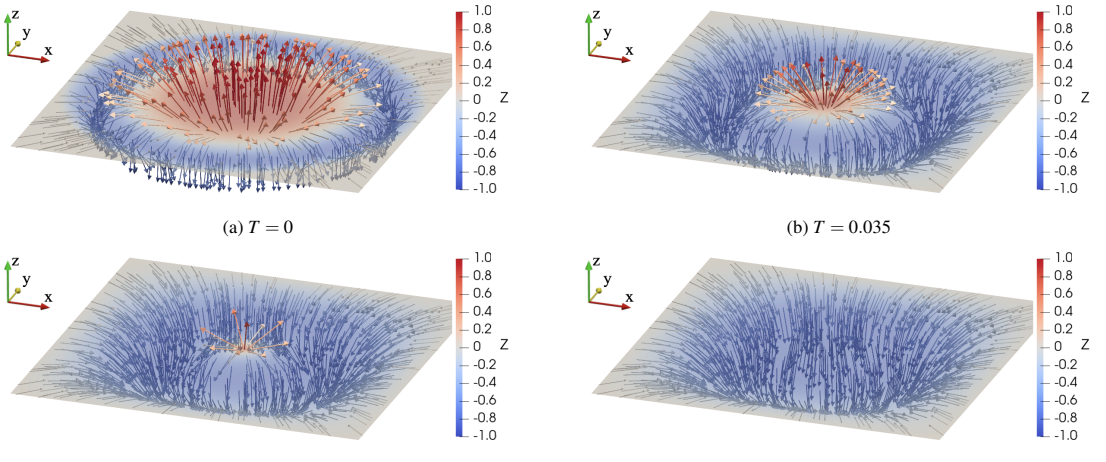

(a) $T = 0$ (b) $T = 0.035$

(c) $T = 0.0576$ (d) $T = 0.0625$

FIG. 4.3. Experiment of Section 4.4: Visualization of numerical solutions computed by the linearized one-stage Gauss method (L^2-gradient flow and $\tau = 2^{-12}$). The arrows illustrate the direction of the vector field, and the color refers to the third component of the vector field, which takes values between -1 (blue) and 1 (red).

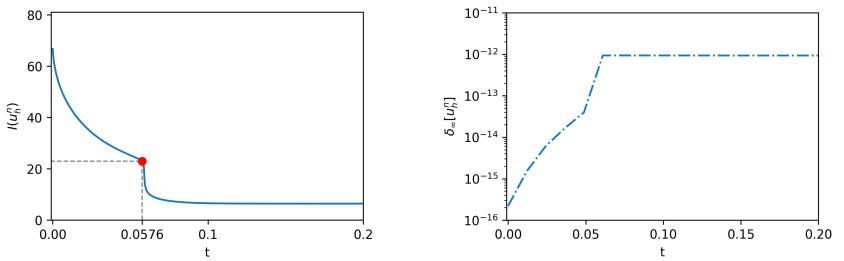

(a) Energy (b) Constraint violation

FIG. 4.4. Experiment of Section 4.4: Evolution of the energy $I(u_h^n)$ (left) and the constraint violation $\delta_\infty[u_h^n]$ (right) for numerical solutions computed by the linearized one-stage Gauss method (L^2-gradient flow and $\tau = 2^{-12}$) for the initial value (4.13).

Acknowledgment

G.A. gratefully acknowledges the support and warm hospitality provided by the Harbin Institute of Technology, Shenzhen, China.

REFERENCES

1. G. Akrivis, S. Bartels, and C. Palus, *Quadratic constraint consistency in the projection-free approximation of harmonic maps and bending isometries*, Math. Comp. **94** (2025) 2251–2269. DOI 10.1090/mcom/4035. MR4919561
2. G. Akrivis, S. Bartels, M. Ruggeri, and J. Wang, *Projection-free approximation of flows of harmonic maps with quadratic constraint accuracy and variable step sizes*, ESAIM Math. Model. Numer. Anal. **60** (2026) 633–655. DOI 10.1051/m2an/2026019.

3. F. Alouges, *A new algorithm for computing liquid crystal stable configurations: the harmonic mapping case*, SIAM J. Numer. Anal. **34** (1997) 1708–1726. DOI 10.1137/S0036142994264249. MR1472192
4. F. Alouges, *A new finite element scheme for Landau-Lifchitz equations*, Discrete Contin. Dyn. Syst. S **1** (2008) 187–196. DOI 10.3934/dcdss.2008.1.187. MR2379897
5. F. Alouges, E. Kritsikis, J. Steiner, and J.-C. Toussaint, *A convergent and precise finite element scheme for Landau–Lifschitz–Gilbert equation*, Numer. Math. **128** (2014) 407–430. DOI 10.1007/s00211-014-0615-3. MR3268842
6. F. Alouges and A. Soyeur, *On global weak solutions for Landau-Lifshitz equations: Existence and nonuniqueness*, Nonlinear Anal. **18** (1992) 1071–1084. DOI 10.1016/0362-546X(92)90196-L. MR1167422
7. R. An, H. Gao, and W. Sun, *Optimal error analysis of Euler and Crank–Nicolson projection finite difference schemes for Landau–Lifshitz equation*, SIAM J. Numer. Anal. **59** (2021) 1639–1662. DOI 10.1137/20M1335431. MR4272916
8. G. Bai, X. Gui, and B. Li, *Convergence of multistep projection methods for harmonic map heat flows into general surfaces*, Numer. Math. **157** (2025) 629–661. DOI 10.1007/s00211-025-01464-9. MR4883780
9. S. Bartels, *Stability and convergence of finite-element approximation schemes for harmonic maps*, SIAM J. Numer. Anal. **43** (2005) 220–238. DOI 10.1137/040606594. MR2177142
10. S. Bartels, Numerical Methods for Nonlinear Partial Differential Equations, volume 47 of Springer Series in Computational Mathematics. Springer, Cham, 2015, pages x+393. DOI 10.1007/978-3-319-13797-1. MR3309171
11. S. Bartels, *Projection-free approximation of geometrically constrained partial differential equations*, Math. Comp. **85** (2016) 1033–1049. DOI 10.1090/mcom/3008. MR3454357
12. S. Bartels, C. Lubich, and A. Prohl, *Convergent discretization of heat and wave map flows to spheres using approximate discrete Lagrange multipliers*, Math. Comp. **78** (2009) 1269–1292. DOI 10.1090/S0025-5718-09-02221-2. MR2501050
13. S. Bartels, C. Palus, and Z. Wang, *Quasi-optimal error estimates for the finite element approximation of stable harmonic maps with nodal constraints*, SIAM J. Numer. Anal. **61** (2023) 1819–1834 DOI 10.1137/22M1524497. MR4615263
14. R. Becker, X. Feng, and A. Prohl, *Finite element approximations of the Ericksen–Leslie model for nematic liquid crystal flow*, SIAM J. Numer. Anal. **46** (2008) 1704–1731. DOI 10.1137/07068254X. MR2399392
15. K. Burrage and J. C. Butcher, *Stability criteria for implicit Runge–Kutta methods*, SIAM J. Numer. Anal. **16** (1979) 46–57. DOI 10.1137/0716004. MR0518683
16. J. C. Butcher, *A stability property of implicit Runge-Kutta methods*, BIT **15** (1975) 358–361. DOI 10.1007/BF01931672.
17. K.-C. Chang, W. Y. Ding, and R. Ye, *Finite-time blow-up of the heat flow of harmonic maps from surfaces*, J. Differ. Geom. **36** (1992) 507–515. DOI euclid.jdg/1214448751. MR1180392
18. G. J. Cooper, *Stability of Runge-Kutta methods for trajectory problems*, IMA J. Numer. Anal. **7** (1987) 1–13. DOI 10.1093/imanum/7.1.1. MR0967831
19. M. Crouzeix, *Sur la B-stabilité des méthodes de Runge-Kutta*, Numer. Math. **32** (1979) 75–82. DOI 10.1007/BF01397651. MR0525638
20. M. Crouzeix, W. H. Hundsdorfer, and M. N. Spijker, *On the existence of solutions of the algebraic equations in implicit Runge–Kutta methods*, BIT **23** (1983) 84–91. DOI 10.1007/BF01937328. MR0689606
21. K. Dekker and J. G. Verwer, Stability of Runge–Kutta Methods for Stiff Nonlinear Differential Equations, North-Holland, Amsterdam, New York, 1984. MR0774402
22. X. Gui, B. Li, and J. Wang, *Convergence of renormalized finite element methods for heat flow of harmonic maps*, SIAM J. Numer. Anal. **60** (2022) 312–338. DOI 10.1137/21M1402212. MR4377027
23. A. Guillou and J. L. Soulé, *La résolution numérique des problèmes différentiels aux conditions initiales par des méthodes de collocation*, Rev. Franç. Inform. Opér. **3** (1969), S'ér. R-3, 17–44. DOI 10.1051/m2an/196903R300171. MR0280008
24. E. Hairer, S. P. Nørsett, and G. Wanner, *Solving Ordinary Differential Equations I: Nonstiff Problems*. Springer Series in Computational Mathematics v. 8, Springer–Verlag, Berlin, 2nd revised ed., 1993, corr. 2nd printing,

2000. DOI 10.1007/978-3-540-78862-1. MR1227985

25. E. Hairer and G. Wanner, *Solving Ordinary Differential Equations II: Stiff and Differential-Algebraic Problems*, volume 14 of Springer Series in Computational Mathematics. Springer-Verlag, Berlin, second rev. edition, 2010, pages xvi+614. DOI 10.1007/978-3-642-05221-7. MR2657217
26. Q. Hu, X.-C. Tai, and R. Winther, *A saddle point approach to the computation of harmonic maps*, SIAM J. Numer. Anal. **47** (2009) 1500–1523. DOI 10.1137/060675575. MR2497338
27. G. Huisken, *Flow by mean curvature of convex surfaces into spheres*, J. Differ. Geom. **20** (1984) 237–266. DOI euclid.jdg/1214438998. MR772132
28. B. Kovács, B. Li, and C. Lubich, *A convergent evolving finite element algorithm for mean curvature flow of closed surfaces*, Numer. Math. **143** (2019) 797–853. DOI 10.1007/s00211-019-01074-2. MR4026373
29. M. Kružík and A. Prohl, *Recent developments in the modeling, analysis, and numerics of ferromagnetism*, SIAM Rev. **48** (2006) 439–483. DOI 10.1137/S0036144504446187. MR2278438
30. F.-H. Lin, *Nonlinear theory of defects in nematic liquid crystals; phase transition and flow phenomena*, Commun. Pure Appl. Math. **42** (1989) 789–814. DOI 10.1002/cpa.3160420605 MR1003435
31. J. Schöberl, *NETGEN An advancing front 2D/3D-mesh generator based on abstract rules*, Comput. Vis. Sci. **1** (1997) 41–52. DOI 10.1007/s007910050004.
32. G. Wanner, *A short proof on nonlinear A-stability*, BIT **16** (1976) 226–227. DOI 10.1007/BF01931374. MR0416037
33. K. Wright, *Some relations between implicit Runge-Kutta, collocation and τ Lanczos methods and their stability properties*, BIT **10** (1970) 217–227. DOI 10.1007/BF01936868. MR0266439